Journal of Magnetism and Magnetic Materials 391 (2015) 166–171

Contents lists available at ScienceDirect

Journal of Magnetism and Magnetic Materials

journal homepage: www.elsevier.com/locate/jmmm

Density Functional Theory applied to magnetic materials: Mn_3O_4 at different hybrid functionals

R.A.P. Ribeiro [a], S.R. de Lazaro [a,*], S.A. Pianaro [b]

[a] Department of Chemistry, State University of Ponta Grossa, Av. General Carlos Cavalcanti, 4748, 84030-900 Ponta Grossa, PR, Brazil
[b] Department of Materials Engineering, State University of Ponta Grossa, Av. General Carlos Cavalcanti, 4748, 84030-900 Ponta Grossa, PR, Brazil

ARTICLE INFO

Article history:
Received 28 September 2014
Received in revised form
2 April 2015
Accepted 22 April 2015
Available online 30 April 2015

Keywords:
DFT
Hybrid functionals
Coupling constants

ABSTRACT

Antiferromagnetic Mn_3O_4 in spinel structure was investigated employing the Density Functional Theory at different hybrid functionals with default HF exchange percentage. Structural, electronic and magnetic properties were examined. Structural results were in agreement with experimental and Hartree–Fock results showing that the octahedral site was distorted by the Jahn–Teller effect, which changed the electron density distribution. Band-gap results for B3LYP and B3PW hybrid functionals were closer to the experimental when compared to PBE0. Mulliken Population Analysis revealed magnetic moments very close to ideal d^4 and d^5 electron configurations of Mn^{3+} and Mn^{2+}, respectively. Electron density maps are useful to determine that oxygen atoms mediate the electron transfer between octahedral and tetrahedral clusters. Magnetic properties were investigated from theoretical results for exchange coupling constants. Intratetrahedral and tetra-octahedral interactions were observed to be antiferromagnetic, whereas, octahedral sites presented antiferromagnetic interactions in the same layer and ferromagnetic in adjacent layers. Results showed that only default B3LYP was successful to describe magnetic properties of antiferromagnetic materials in agreement with experimental results.

1. Introduction

Materials with spinel structure have important technological applications, such as gas sensors, electrical and magnetic materials, and other electronic devices. The spinel structure presents AB_2O_4 formula where cations A^{2+} and B^{3+} occupy tetrahedral and octahedral sites, respectively. Such cations (A, B) can be mixed, as for the ternary spinels ($MgAl_2O_4$), or correspond to the same metal with different valences (2+ and 3+), for instance Mn_3O_4 [1–4]. These materials have high scientific and technological interest due to their structural and magnetic properties, which allow the development of theoretical and experimental investigations [5–7]. In recent years, a lot of theoretical studies have been developed to investigate the structural, electronic and magnetic properties of materials with spinel structure such as Co_3O_4, Fe_3O_4, Fe_3S_4, Mn_3O_4, showing good agreement with experimental results [8–11].

Hausmannite (Mn_3O_4) is a material with normal spinel structure that has the tetrahedral sites occupied by the cation Mn^{2+} and the octahedral sites by Mn^{3+} cations. This structure has lattice parameters $a=b=5.7474$ Å and $c=9.457$ Å in a tetragonal arrangement with space group *I41/amd* (Fig. 1). This material presents the octahedral sites distorted by the Jahn–Teller effect due to the electronic configuration of the cation Mn^{3+} (d^4) which enables partial occupation of e_g and t_{2g} levels. In recent years, this material has attracted interest for its technological applications as insertion in lithium ion batteries, electrochemical processes, supercapacitors, catalysts for environmental applications, and others [12–18].

Antiferromagnetic oxides such as Mn_3O_4 have antiparallel alignment between non-equivalent sublattices occupied by different cations. These couplings are mediated by oxygen atoms that coordinate with cations of different sites, and the geometric and electronic distribution of these cations changes the magnitude of these interactions [19]. In Mn_3O_4 material the predominant exchanges are J_{AA}, J_{BB} and J_{AB}, where A and B are the cations distributed in tetrahedral and octahedral sites, respectively [20,21]. In Hausmannite, due to Jahn–Teller effect, the octahedral site is distorted and the exchange coupling constants for this lattice is divided into interactions in and out of plane (J_{BB-p} and J_{BB-op}). Therefore, the exchange coupling in the plane is more intense than out of the plane ($J_{BB-p} > J_{BB-op}$) and these are more intense than the exchange coupling in tetrahedral lattice [20–24]. These exchange couplings provide a lot of the magnetic transitions and below $T_N=41.2$ K these materials have Yafet–Kittel ferrimagnetic structure [25].

Theoretical studies on Mn_3O_4 previously developed report the

* Corresponding author.
E-mail address: srlazaro@upeg.br (S.R. de Lazaro).

http://dx.doi.org/10.1016/j.jmmm.2015.04.091
0304-8853/

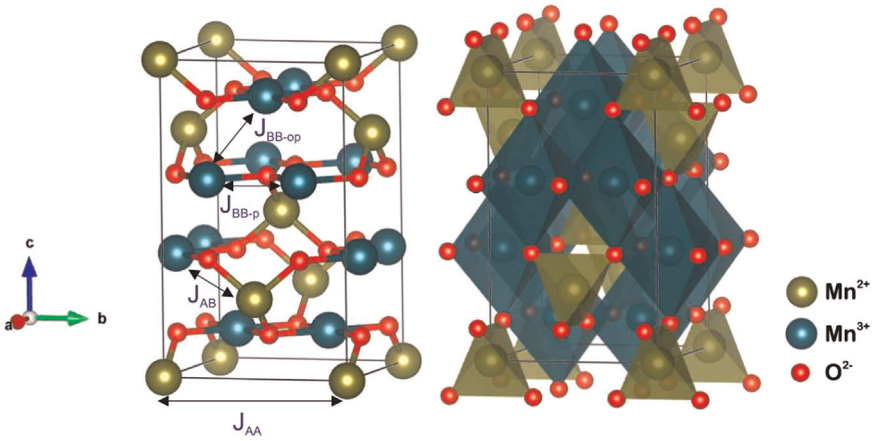

Fig. 1. Unit cell for Mn_3O_4 material. Blue and green polyhedral represent octahedral [MnO_6] and tetrahedral [MnO_4] clusters, respectively. (For interpretation of the references to color in this figure legend, the reader is referred to the web version of this article.)

use of computational methods to describe the structural, electronic and magnetic properties of this material in agreement with experimental results [26,27]. Chartier and coworkers investigated the exchange coupling constants for Mn_3O_4 at Hartree–Fock level and noted that this methodology has a deviation around 40–50% in comparison to experimental results [26]. Franchini and co-authors performed Density Functional Theory (DFT) calculations using gradient corrected functionals, as PBE, PBE+U and hybrids PBE0 and HSE to investigate the ground-state properties of multivalent manganese oxides (MnO, Mn_3O_4, α-Mn_2O_3, β-MnO_2) and pointed out that hybrid functionals appear to provide a better description for these properties [27]. However, the obtained theoretical predictions for the magnetic properties did not approach the experimental results due to the use of functionals which presented severe limitations to describe this behavior making it necessary to clarify the exchange-correlation functional effect on the magnetic properties of materials. Recently, a lot of studies have involved a class of functional, which incorporates a fraction of the Hartree–Fock exchange to better describe the properties of different materials that have been denominated hybrid functional. A large number of hybrid functionals are described in the literature for different types of applications [28,29]. In particular, the B3LYP functional and B3PW are characterized by presenting a non-local exchange functional developed by Becke combined with a correlation functional based on gradient of electronic density developed by Lee et al. and Perdew and Wang, respectively [30–32]. Already the PBE functional is a parameterization defined by Perdew–Burke–Ernzerhof for the generalized gradient approximation (GGA), which was extended into a functional hybrid with a optimum value of 25% for HF exchange termed as PBE0 [33–35]. However, several literature reports suggest that this percentage is not a good choice to represent band-gaps and other ground-state properties of solid state materials [35–38]. In recent years, these functionals began to be used for representing the magnetic properties of different materials [39,40]. Some of these studies have reported strong dependence of the results in relation to exchange coupling constants and the fraction of HF exchange incorporated into hybrid functionals. Feng and coworkers [41] confirmed the percentage of 35% as optimal for the correct description of the magnetic property using hybrid B3LYP functional [42]. Another work discussed that such dependence can be overcome by the replacement of these adjusted functionals for Heyd–Scuseria–Ernzerhof (HSE) hybrid approach or advanced variational pseudo-self-interaction correction method [43]. Recently, a lot of theoretical studies have been developed using DFT+U methodology mainly for magnetic properties predictions [44–46]. Nevertheless, the choice of Hubbard parameters is often arbitrary, although it drastically affects physical properties [47]. Furthermore, the hybrid functionals have the advantage that the self-interaction corrections are included at the same footing for every orbitals and not as the multiorbital model for DFT+U enabling to treat non-local effects through the non-local HartreeFock exact exchange [35]. However, our results prove that, despite the theoretical evidences of 35% fraction of HF exchange being necessary for a correct description of the magnetic properties, B3LYP hybrid functional with default HF percentage (25%) provide an excellent description for ground-state properties of antiferromagnetic materials.

2. Computational methodology

Computer simulations were performed using the Density Functional Theory with the hybrid functionals B3LYP, B3PW and PBE0 implemented in software CRYSTAL09 [30,31,48]. The unit cell, shown in Fig. 1, with space group *I41/amd* was based on the experimental lattice parameters $a=b=5.7474$ Å and $c=9.457$ Å and internal coordinates: Mn^{2+} (0; 0,250; 0,875), Mn^{3+} (0; 0,5; 0,5) and O^{2-} (0; 0,484; 0,255) [49]. Mn and O atoms were represented by Mn-86-411d41G and 8411d1 basis sets, respectively [50]. The Mn_3O_4 unit cell presented two Mn^{2+} (d^5) and four Mn^{3+} (d^4) cations allowing the representation as a ferromagnetic model (FEM) in a setting where the cations of the tetrahedral and octahedral sites have electrons in spin up configuration (↑ ↑ ↑ ↑ ↑ ↑ ↑). For this model, the total energy was optimized in relation to the structural parameters and, later on, compared to experimental results [49]. The electronic structure was investigated by analysis of the Density of States and Charge Density Maps, as well as Mulliken Population Analysis for the electron spins. These results were obtained from optimized wave function, whereas, the convergence criteria to mono-and bielectronic integrals was truncated in 10^{-8} Hartree, with Shrinking factor set to 4×4 (Gilat Web) corresponding to 13 independent k points in the Brillouin zone according to the Monkhorst–Pack method [51]. The processor used was an AMD Phenom Quad-Core 64-bits.

To evaluate the magnetic interactions between cations of different sites in the Mn_3O_4 material, six ferrimagnetic models were designed: $FIM_1 = (\downarrow\downarrow\uparrow\uparrow\uparrow\uparrow\uparrow)$, $FIM_2 = (\uparrow\downarrow\uparrow\uparrow\uparrow\uparrow\uparrow)$, $FIM_3 = (\uparrow\uparrow\downarrow\downarrow\uparrow\uparrow\uparrow)$, $FIM_4 = (\uparrow\uparrow\uparrow\downarrow\uparrow\downarrow)$, $FIM_5 = (\uparrow\uparrow\downarrow\uparrow\uparrow\uparrow\uparrow)$ and $FIM_6 = (\uparrow\uparrow\downarrow\uparrow\downarrow\uparrow\downarrow)$ as proposed by Chartier and co-authors [26]. The theoretical Total Energies obtained for these models are presented in Table 1. In these calculations the unit cell of FIM configurations correspond to the FEM optimized geometry. The optimization process was performed only for FEM model because ferrimagnetic models have low symmetry and, consequently, higher computational cost. In the Solid State Theory, the

Table 1
Total Energies (in Hartree) for the ferromagnetic (FEM) and ferrimagnetic (FIM) models of the Mn_3O_4 material at different hybrid functionals.

Models	B3LYP	B3PW	PBE0
FEM	−7507.90872889	−7508.20302609	−7506.70358883
FIM1	−7507.91270469	−7508.22986121	−7506.69985071
FIM2	−7507.91341374	−7508.21862759	−7506.70348420
FIM3	−7507.90072507	−7508.21634243	−7506.70202282
FIM4	−7507.92182178	−7508.20762781	−7506.69302183
FIM5	−7507.91277741	−7508.20530164	−7506.69838109
FIM6	−7507.92352478	−7508.20310297	−7506.69572080

magnetic interactions are usually described by the Heisenberg Hamiltonian; however, in computer simulations such a relationship cannot be used because the Slater determinant is not an eigenstate of the Heisenberg Hamiltonian requiring the application of the Ising model. This model allows to relate the coupling constants J with the energy difference of the magnetic states since the unpaired electrons are well defined [41,52]. This model can be described by the equations:

$$\hat{H}_{sing} = \sum J_{ij} . \hat{S}_{iz} . \hat{S}_{jz} \quad (1)$$

$$\Delta E_{FIM-FEM} = -2 \sum Z_{ij} . S_i . S_j . J_{ij} \quad (2)$$

Eqs. (1) and (2) involve the number of neighbors i–j (Z), the electronic spin of different species (S) and coupling constant between the species (J). The summation usually extends to first or second neighbors i–j, where i and j correspond to different magnetic sites, without double counting. This proposal can be applied to the six models previously proposed and the coupling constants (J_{AA}, J_{AB}, J_{BB-p} and J_{BB-op}) can be calculated from the equations using the Total Energies presented in Table 1:

$$\Delta E_1 = -48 J_{AB} S_A S_B \quad (3)$$

$$\Delta E_2 = 24 J_{AB} S_A S_B + 8 J_{AA} S_A^2 \quad (4)$$

$$\Delta E_3 = 24 J_{AB} S_A S_B + 16 J_{BBl} S_B^2 \quad (5)$$

$$\Delta E_4 = 24 J_{AB} S_A S_B + (8 J_{BBl} + 4 J_{BBs}) S_B^2 \quad (6)$$

$$\Delta E_5 = 12 J_{AB} S_A S_B + (8 J_{BBl} + 4 J_{BBs}) S_B^2 \quad (7)$$

$$\Delta E_5 = 8 J_{AA} S_A^2 + 12 J_{AB} S_A S_B + (8 J_{BBl} + 4 J_{BBs}) S_B^2 \quad (8)$$

3. Results and discussions

3.1. Structural parameters

Theoretical and experimental results for the structural parameters of ferromagnetic model for Mn_3O_4 material are shown in Table 2. Results obtained from Density Functional Theory (DFT) simulations with different hybrid functionals were observed to be in agreement with other theoretical [26] and experimental [49] results.

Bond length and bond angles (Table 2) show a distorted crystalline structure for the Mn_3O_4. Such distortions are identified at the octahedral site through different bond lengths, represented by Mn–O_{eq} and Mn–O_{ax} bond length and the bond angles deviation from the ideal angle of 90°. In relation to the tetrahedral site, the four obtained Mn–O bond lengths are equal; however, the bond angles were deviated from the ideal angle of 109.47°.These distortions occur because of the Jahn–Teller effect causing alterations in the intrasites distance, more specifically, between cation neighbors localized in the octa- and tetrahedral sites (4.02 and 4.30 Å), therefore, the magnetic couplings between these sites are influenced. Regarding the different methodologies, it was observed that the hybrid functionals employed in this work were satisfactorily accurate with respect to structural experimental results.

3.2. Electronic structure

Electronic properties were investigated using DOS, Mulliken Population Analysis and Charge Density Maps obtained from optimized wave function. From total and atom-resolved DOS projected, as shown in Fig. 2, the valence band (VB) was observed to be composed mostly of atomic states from oxygen (2p) and the Mn (3d) in the octahedral site. In relation to the conduction band (CB) composition, a predominant contribution of Mn (3d) of octa- and tetrahedral sites was observed. Thus, it is possible to assume that an electron transfer inside band-gap region should occur between the 2p orbitals of the oxygen atom and 3d orbitals of the Mn atom in the octahedral site, which presented d^4 configuration. From DOS results the band-gap was calculated as 3.02, 2.69 and 2.61 eV for PBE0, B3PW and B3LYP hybrid functionals, respectively, indicating the B3LYP hybrid functional as the best representation for optical property and it is in good agreement with experimental results (2.30–2.50 eV) [53]. This behavior was also observed for other materials [29]. For hybrid functionals, the HF exchange energy is mixed into the total energy functional of GGA and the weights of correlation, local exchange and non-local HF exchange energies can be determined by a fitting of theoretical thermochemical properties (atomization energies, ionization potentials, proton affinities and total atomic energy) from experimental results [27,30]. In band-gap calculations, this process is essential to achieve better results especially because the ionization potential is related to the electron orbital energies; however, PBE0 is a hybrid functional with a predefined amount of the exact exchange. For this reason the band-gaps calculated from B3PW and B3LYP hybrid functionals were in better agreement with experimental results. In comparison to the band-gap calculated by Franchini and co-workers [27] using PBE0 hybrid functional (2.4 eV), it was observed that Gaussian basis set jointly PBE0 hybrid functional, used in this work, induces an overestimation of band-gap in relation to plane-waves/PBE0 combination.

To analyze the electronic distribution in the molecular structure of Mn_3O_4 Mulliken Population Analysis applied to atomic charge and spin state was used, as shown in Table 3. Nevertheless, such theoretical results depend on the atomic basis set; then, the discussion about charge net will be performed through a qualitative viewpoint. The calculated charge for the Mn atom in tetrahedral site was observed to be in accordance with the formal charge Mn^{2+} and the remaining values did not approach the formal values of +3 and −2 for the octahedral manganese and oxygen atoms, respectively. Regarding spin distribution, the total values resembled the d^4 and d^5 electronic configurations for Mn^{2+} and Mn^{3+} atoms, respectively, confirming the ferromagnetic state (FEM model) for Mn_3O_4 material. Nevertheless, for each Mn^{2+} atom (tetrahedral site), the spin occupation in 3d orbital corresponded to approximately one electron unpaired in agreement with d^5 electronic configuration; whereas, for Mn^{3+} (octahedral site) were observed $3d_{xy}$, $3d_{xz}$, $3d_{yz}$, $3d_{z^2}$, orbitals with spin occupation of approximately one electron were observed, as a $3d^4$ and $3d_{x^2y^2}$ orbital had spin occupation close to zero. This difference between spin distributions on Mn atoms shows a shortening of the

Table 2
Theoretical and experimental results for lattice parameters (in Å) of the Mn_3O_4 material. Mn–O_{eq} and Mn–O_{ax} correspond to equatorial and axial bond distances between manganese and oxygen atoms for different sites. The angles α and β refer to O_{ax}–Mn–O_{eq} and O_{eq}–Mn–O_{eq} angles in the octahedral site. γ and δ represent the angles for tetrahedral site angles.

	Lattice parameters		Octahedral				Tetrahedral		
	$a=b$	c	Mn–O_{eq}	Mn–O_{ax}	α	β	Mn–O	γ	δ
PBE0	5.794	9.470	1.935	2.299	95.35	97.11	2.049	104.17	112.18
B3PW	5.803	9.498	1.938	2.311	95.67	97.22	2.049	104.21	112.25
B3LYP	5.901	9.394	1.959	2.307	95.24	97.16	2.065	104.14	112.20
HF [26]	5.919	9.311	1.956	2.247	96.54	98.53	2.098	106.65	110.90
Exp. [49]	5.747	9.457	1.945	2.288	94.68	95.60	2.011	102.75	112.93

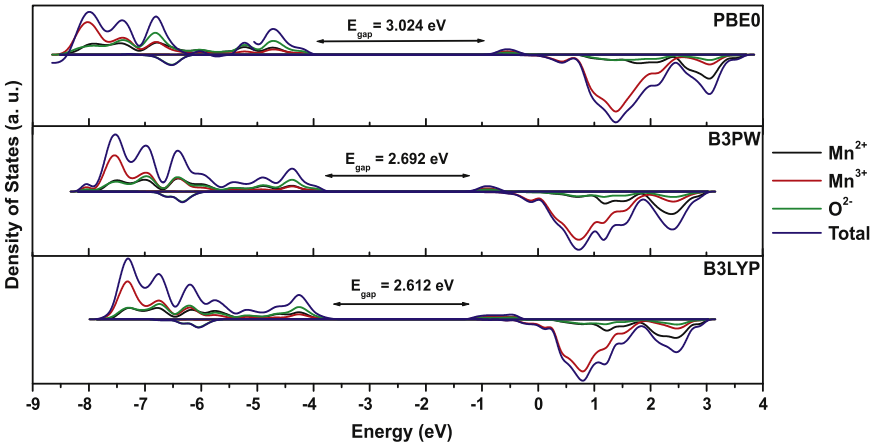

Fig. 2. Total and atom-resolved Density of States for Mn_3O_4 material which PBE0, B3PW and B3LYP hybrid functional.

equatorial bond distances in the octahedron site due to the influence on e_g level characterizing a JahnTeller distortion. The results obtained are very similar to other theoretical predictions of ferrites with spinel structure [54]. Furthermore, no significant change was noted between hybrid functionals and Mulliken Population results.

The Charge Density Maps analysis in [111] direction (Fig. 3) provided relevant information in relation to charge connection between [MnO_6] and [MnO_4]clusters and such direction was chosen because it made possible to analyze both clusters simultaneously. It was observed that the electronic distribution around the [MnO_6] cluster had approximately cylindrical structure failure because the $3d_{x^2y^2}$ orbital was not filled providing the elongation of Mn–O bond distance in the axial plane; consequently, there was a decrease in electronic overlap of this bond. For the [MnO_4] cluster, the charge distribution presented distortion in the z direction, which was efficient to connect this cluster to [MnO_6] cluster. Thus, the antiferromagnetic property in the Mn_3O_4 material originated from the charge connection described between [MnO_6] and [MnO_4] clusters determined the modification in the spin coupling.

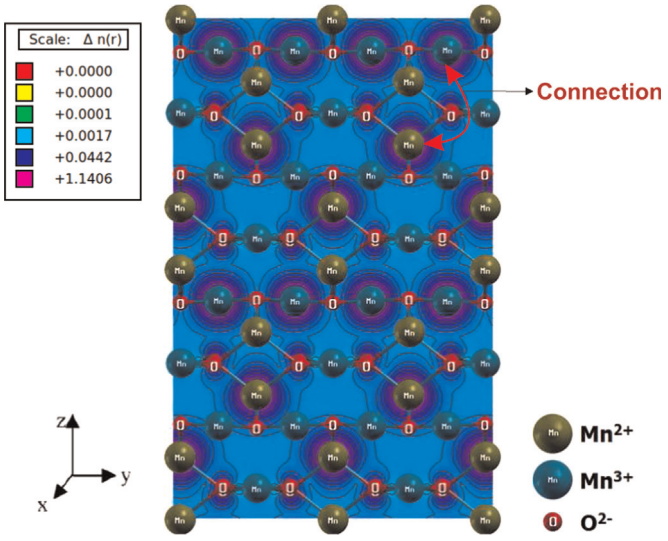

Fig. 3. Electron Density Map in [111] direction for Mn_3O_4 material. The charge connection between [MnO_6] and [MnO_4] clusters is indicated for double narrow.

3.3. Exchange coupling

As described in Section 2, in general, the information on the signal and magnitude of the magnetic coupling (J) among octa- and octahedral sites, tetra and tetrahedral sites and octa- and tetrahedral sites can be extracted performing simulations with unpaired electrons localized on Mn atoms to compute the ferrimagnetic structure total energy (Table 1). The Mn_3O_4 material exhibits a noncollinear ferrimagnetic ground state, but due to the high computational cost required for these propose we only consider collinear models. In relation to the Total Energies of FEM and FIM models, it was observed that for B3LYP and B3PW hybrid functionals the ferrimagnetic configurations were more stable than the ferromagnetic model. However, the most stable configuration was different at these functionals with FIM6 and FIM1 corresponding to the ground-state at B3LYP and B3PW, respectively. This difference can be attributed to the different Hamiltonian proposed in these functionals, i.e. the different treatment of correlation energy by Perdew–Wang (B3PW) and Lee–Yang–Parr (B3LYP) expressions affects the stabilization of different magnetic states of solid materials. The PBE0 ferromagnetic phase was observed to be the most stable configuration Mn_3O_4 unlike

Table 3
Theoretical results of the Mulliken Population Analysis for charge net (in |e|) and spin net of Mn_3O_4 material performed on different hybrid functional.

	Mn^{2+}			Mn^{3+}			O		
	B3LYP	B3PW	PBE0	B3LYP	B3PW	PBE0	B3LYP	B3PW	PBE0
$3d_{xy}$	0.964	0.965	0.968	0.872	0.874	0.879	–	–	–
$3d_{xz}$	0.917	0.919	0.925	0.937	0.945	0.942	–	–	–
$3d_{yz}$	0.917	0.919	0.925	0.944	0.938	0.949	–	–	–
$3d_{z2}$	0.935	0.937	0.942	0.925	0.926	0.930	–	–	–
$3d_{x2y2}$	0.965	0.955	0.970	0.195	0.204	0.201	–	–	–
Spin net	4.726	4.738	4.760	3.898	3.920	3.930	0.119	0.106	0.095
Charge net	1.709	1.722	1.856	1.856	1.862	1.889	−1.355	−1.362	−1.378

Table 4
Exchange coupling constants (K) of Mn_3O_4 material for different hybrid functional.

	B3LYP	B3PW	PBE0	HF [26]	Exp. [21]
J_{AA}	−5.73	−38.02	5.26	-4.13	−4.9
J_{AB}	−20.01	−15.36	−12.79	−3.11	−6.8
J_{BB-op}	50.35	0.52	−1.49	4.95	–
J_{BB-p}	−162.27	90.06	87.02	−29.7	–
J_{BB}	−20.52	30.37	28.01	−6.57	−19.9

experimental observations of a noncollinear ferrimagnetic behavior and PBE0 calculations developed by Franchini and coworkers [27]. In comparison to these theoretical results, it was seen that the atomic orbitals basis set based on Gaussian description combined with the PBE0 hybrid functional used in this work is not a good choice to the treatment of magnetic materials because it reproduces erroneously the equilibrium state of these materials.

Theoretical and experimental results for exchange coupling constant for Mn_3O_4 are shown in Table 4. In relation to interpretation, theoretical results with negative signal indicated an antiferromagnetic coupling, whereas, positive signal evidenced a ferromagnetic coupling between atoms. Thus, from these theoretical results it was observed that B3LYP hybrid functional showed a better agreement with experimental results, where the magnetic interactions in the same site (J_{AA} and J_{BB}) were better described than exchange constants for atoms in different sites (J_{AB}). Furthermore, the B3LYP hybrid functional also described better magnetic behavior for complex oxides compared to B3PW, PBE0 and Hartree–Fock results. The nature of the exchange coupling constants for B3LYP functional indicated an antiferromagnetic interaction between tetra-tetrahedral manganese (J_{AA}) and tetra-octahedral manganese (J_{AB}). In the octahedral site, manganese atoms with different bond length were noticed (Table 2) due to Jahn–Teller distortions causing distorted [MnO_6] clusters; however, for the neighbor atoms located at short distances (J_{BB-p}) in the octahedral plane there was antiferromagnetic interaction, whereas, for octahedral out-plane neighbors (J_{BB-op}) ferromagnetic interaction was observed. Therefore, the octahedral sites have antiparallel spin alignment in the same layer, whereas, for adjacent layers the spins are aligned in parallel.

UHF underestimation arising as a consequence of correlation effects are not included in the theoretical formalism, leading to large on-site Coulomb interactions and small magnetic coupling constant, making hybrid functionals formalism the best candidates for the electronic behavior of magnetic material description. Furthermore, Franchini and coworkers suggest that the default percentage of HF exchange used in hybrid functionals is not an optimum parameter for studying magnetic properties of materials [27]. However, the theoretical results shown in Table 4 indicated that default B3LYP hybrid functional used in this work (20% HF exchange) reproduced efficiently magnetic coupling constant for Mn_3O_4 material, while B3PW and PBE0 functionals exhibited larger discrepancies at the same parameters. Furthermore, hybrid functionals might need adjustment at HF exchange term to better reproduce exchange coupling results in antiferromagnetic semiconductors. Our results showed that B3LYP functional is a successful hybrid functional to describe magnetic properties of antiferromagnetic materials due to self-interaction reduction caused by percentage used at HF exchange term, whereas, for B3PW and PBE0 functionals different percentage of HF exchange might be required.

4. Conclusions

This study showed that hybrid Density Functional Theory applied to antiferromagnetic Mn_3O_4 in spinel structure is a suitable tool to investigate material structural, electronic and magnetic properties. For structural properties the lattice parameters and bond distances calculated were in agreement to experimental results. These results indicated that the octahedral site was distorted by the Jahn–Teller effect. Results for electronic properties indicated that B3LYP hybrid functional provided the best description of band-gap for Mn_3O_4 as for other kinds of materials [55,56]. Mulliken Population Analysis and Electron Density Maps revealed that Mn^{2+} had a spherical structure distorted in z direction for electron density and Mn^{3+} had a cylindrical structure due the partial filling of 3d orbitals which led to Jahn–Teller effect. Furthermore, it could be seen that these clusters were connected by oxygen atoms that mediated the electron transfer. Regarding magnetic properties, the calculated coupling constants were observed to indicate that the octahedral site had antiparallel spin alignment in the same layer and parallel spin alignment in adjacent layers and that for tetrahedral site the spin alignment was antiparallel as proved in the literature. From these theoretical results, it was observed that Density Functional Theory allied to hybrid functional provided the best description for exchange parameters in relation the Hartree–Fock level due to incorporation of correlation effects. However, when comparing B3LYP, B3PW and PBE0 hybrid functionals, only B3LYP produced theoretical results close to experimental, confirming that this functional can describe antiferromagnetic materials successfully with a default percentage of HF exchange.

Acknowledgments

This work was supported by UEPG, CAPES and Fundação Araucária.

References

[1] D. Jnaneshwara, D. Avadhani, B.D. Prasad, B. Nagabhushana, H. Nagabhushana, S. Sharma, C. Shivakumara, J. Rao, N. Gopal, S.-C. Ke, R. Chakradhar, Electron paramagnetic resonance, magnetic and electrical properties of $CoFe_2O_4$ nanoparticles, J. Magn. Magn. Mater. 339 (2013) 40–45 http://dx.doi.org/10.1016/j.jmmm.2013.02.028.

[2] C. Xiangfeng, L. Xingqin, M. Guangyao, Effects of CdO dopant on the gas sensitivity properties of $ZnFe_2O_4$ semiconductors, Sens. Actuators B 65 (1–3) (2000) 64–67 http://dx.doi.org/10.1016/S0925-4005(99)00430-X.

[3] S.-W. Han, J.H. Ryu, J. Jeong, D.-H. Yoon, Solid-state synthesis of $Li_4Ti_5O_{12}$ for high power lithium ion battery applications, J. Alloy. Compd. 570 (2013) 144–149 http://dx.doi.org/10.1016/j.jallcom.2013.03.203.

[4] R.M.A. Roque-Malherbe, The Physical Chemistry of Materials: Energy and Environmental Applications, 1st ed., Taylor & Francis, Boca Raton, 2010.

[5] I. Ciofini, C.A. Daul, DFT calculations of molecular magnetic properties of coordination compounds, Coord. Chem. Rev. 238–239 (2003) 187–209 http://dx.doi.org/10.1016/S0010-8545(02)00330-2.

[6] T.T. Nguyen, T.C. Bach, H.T. Pham, T.T. Pham, D.T. Nguyen, N.N. Hoang, Magnetic state of the bulk, surface and nanoclusters of $CaMnO_3$: a DFT study, Physica B 406 (19) (2011) 3613–3621 http://dx.doi.org/10.1016/j.physb.2011.06.054.

[7] F. Wang, W.-W. Huang, S.-Y. Li, A.-Q. Lian, X.-T. Zhang, W. Cao, The magnetic properties of $Fe_xZn_{1-x}O$ synthesized via the solid-state reaction route: experiment and theory, J. Magn. Magn. Mater. 340 (2013) 5–9 http://dx.doi.org/10.1016/j.jmmm.2013.03.026.

[8] X.-L. Xu, Z.-H. Chen, Y. Li, W.-K. Chen, J.-Q. Li, Bulk and surface properties of spinel Co_3O_4 by density functional calculations, Surf. Sci. 603 (4) (2009) 653–658 http://dx.doi.org/10.1016/j.susc.2008.12.036.

[9] B. Siberchicot, On the optical properties and low pressure-induced spin transition in magnetite from ab initio calculations, J. Magn. Magn. Mater. 335 (2013) 86–89 http://dx.doi.org/10.1016/j.jmmm.2012.12.026.

[10] A. Roldan, D. Santos-Carballal, N.H. de Leeuw, A comparative DFT study of the mechanical and electronic properties of greigite Fe_3S_4 and magnetite Fe_3O_4, J. Chem. Phys. 138 (20) (2013) 204712 http://dx.doi.org/10.1063/1.4807614.

[11] C. Franchini, J. Zabloudil, R. Podloucky, F. Allegretti, F. Li, S. Surnev, F.P. Netzer, Interplay between magnetic, electronic, and vibrational effects in monolayer Mn_3O_4 grown on Pd(100), J. Chem. Phys. 130 (12) (2009) 124707 http://dx.doi.org/10.1063/1.3097957.

[12] J.B. Goodenough, A.L. Loeb, Theory of ionic ordering, crystal distortion, and magnetic exchange due to covalent forces in spinels, Phys. Rev. 98 (1955) 391–408, http://dx.doi.org/10.1103/PhysRev.98.391.

[13] T. Suzuki, K. Adachi, T. Katsufuji, Coupling between magnetic, dielectric properties and crystal structure in MnT_2O_4 (T=V, Cr, Mn), J. Phys.: Conf. Ser. 31 (1) (2006) 235–236.

[14] H. Wang, L.-F. Cui, Y. Yang, H. Sanchez Casalongue, J.T. Robinson, Y. Liang, Y. Cui, H. Dai, Mn_3O_4-graphene hybrid as a high-capacity anode material for lithium ion batteries, J. Am. Chem. Soc. 132 (40) (2010) 13978–13980, http://dx.doi.org/10.1021/ja105296a.

[15] P. Li, C. Nan, Z. Wei, J. Lu, Q. Peng, Y. Li, Mn_3O_4 nanocrystals: facile synthesis, controlled assembly, and application, Chem. Mater. 22 (14) (2010) 4232–4236, http://dx.doi.org/10.1021/cm100831q.

[16] W. Gao, S. Ye, M. Shao, Solution-combusting preparation of mono-dispersed Mn_3O_4 nanoparticles for electrochemical applications, J. Phys. Chem. Solids 72 (9) (2011) 1027–1031 http://dx.doi.org/10.1016/j.jpcs.2011.05.015.

[17] G.S. Gund, D.P. Dubal, B.H. Patil, S.S. Shinde, C.D. Lokhande, Enhanced activity of chemically synthesized hybrid graphene oxide/Mn_3O_4 composite for high performance supercapacitors, Electrochim. Acta 92 (2013) 205–215 http://dx.doi.org/10.1016/j.electacta.2012.12.120.

[18] Y. Yao, C. Xu, S. Yu, D. Zhang, S. Wang, Facile synthesis of Mn_3O_4-reduced graphene oxide hybrids for catalytic decomposition of aqueous organics, Ind. Eng. Chem. Res. 52 (10) (2013) 3637–3645, http://dx.doi.org/10.1021/ie303220x.

[19] D. Fiorani, Surface Effects in Magnetic Nanoparticles, Springer, New York, 2005.

[20] K. Kuo, C.W. Cheng, G. Chern, The magnetic Curie temperature and exchange coupling between cations in tetragonal spinel oxide $Mn_{2.5}M_{0.5}O_4$ (M=Co, Ni, Mn, Cr, and Mg) films, J. Appl. Phys. 111 (7) (2012) 07A507 http://dx.doi.org/10.1063/1.3672407.

[21] Y. Nii, H. Sagayama, H. Umetsu, N. Abe, K. Taniguchi, T. Arima, Interplay among spin, orbital, and lattice degrees of freedom in a frustrated spinel Mn_3O_4, Phys. Rev. B 87 (2013) 195115, http://dx.doi.org/10.1103/PhysRevB.87.195115.

[22] J.-H. Chung, J.-H. Kim, S.-H. Lee, T.J. Sato, T. Suzuki, M. Katsumura, T. Katsufuji, Magnetic excitations and orbital physics in the ferrimagnetic spinels MnB_2O_4 (B=Mn, V), Phys. Rev. B 77 (2008) 054412, http://dx.doi.org/10.1103/PhysRevB.77.054412.

[23] J.-H. Chung, K. Hwan Lee, Y.-S. Song, T. Suzuki, T. Katsufuji, Low temperature structural instability of tetragonal spinel Mn_3O_4, J. Phys. Soc. Jpn. 82 (3) (2013) 034707, http://dx.doi.org/10.7566/JPSJ.82.034707.

[24] G. Srinivasan, M.S. Seehra, Magnetic properties of Mn_3O_4 and a solution of the canted-spin problem, Phys. Rev. B 28 (1983) 1–7, http://dx.doi.org/10.1103/PhysRevB.28.1.

[25] Y. Yafet, C. Kittel, Antiferromagnetic arrangements in ferrites, Phys. Rev. 87 (1952) 290–294, http://dx.doi.org/10.1103/PhysRev.87.290.

[26] A. Chartier, P. D'Arco, R. Dovesi, V.R. Saunders, An ab initio Hartree–Fock investigation of the structural, electronic and magnetic properties of Mn_3O_4, Phys. Rev. B 60 (1999) 14042–14048, http://dx.doi.org/10.1103/PhysRevB.60.14042.

[27] C. Franchini, R. Podloucky, J. Paier, M. Marsman, G. Kresse, Ground-state properties of multivalent manganese oxides: density functional and hybrid density functional calculations, Phys. Rev. B 75 (2007) 195128, http://dx.doi.org/10.1103/PhysRevB.75.195128.

[28] Z.-y. Chen, J.-l. Yang, The B3LYP hybrid density functional study on solids, Front. Phys. China 1 (3) (2006) 339–343, http://dx.doi.org/10.1007/s11467-006-0026-8.

[29] J. Muscat, A. Wander, N. Harrison, On the prediction of band gaps from hybrid functional theory, Chem. Phys. Lett. 342 (3–4) (2001) 397–401 http://dx.doi.org/10.1016/S0009-2614(01)00616-9.

[30] A.D. Becke, Density-functional thermochemistry. III. The role of exact exchange, J. Chem. Phys. 98 (7) (1993) 5648–5652 http://dx.doi.org/10.1063/1.464913.

[31] C. Lee, W. Yang, R.G. Parr, Development of the Colle-Salvetti correlation-energy formula into a functional of the electron density, Phys. Rev. B 37 (1988) 785–789, http://dx.doi.org/10.1103/PhysRevB.37.785.

[32] J.P. Perdew, Y. Wang, Accurate and simple density functional for the electronic exchange energy: generalized gradient approximation, Phys. Rev. B 33 (1986) 8800–8802, http://dx.doi.org/10.1103/PhysRevB.33.8800.

[33] J.P. Perdew, K. Burke, M. Ernzerhof, Generalized gradient approximation made simple, Phys. Rev. Lett. 77 (1996) 3865–3868, http://dx.doi.org/10.1103/PhysRevLett.77.3865.

[34] C. Adamo, V. Barone, Toward reliable density functional methods without adjustable parameters: the PBE0 model, J. Chem. Phys. 110 (13) (1999) 6158–6170 http://dx.doi.org/10.1063/1.478522.

[35] C. Franchini, Hybrid functionals applied to perovskites, J. Phys.: Condens. Matter 26 (25) (2014) 253202, http://dx.doi.org/10.1088/0953-8984/26/25/253202.

[36] J.E. Moussa, P.A. Schultz, J.R. Chelikowsky, Analysis of the Heyd–Scuseria–Ernzerhof density functional parameter space, J. Chem. Phys. 136 (20) (2012) 204117, http://dx.doi.org/10.1063/1.4722993.

[37] J. He, C. Franchini, Screened hybrid functional applied to $3d^0$–$3d^8$ transition-metal perovskites $LaMO_3$ (M=ScCu): influence of the exchange mixing parameter on the structural, electronic, and magnetic properties, Phys. Rev. B 86 (23) (2012) 235117, http://dx.doi.org/10.1103/PhysRevB.86.235117.

[38] A. Alkauskas, P. Broqvist, A. Pasquarello, Defect levels through hybrid density functionals: insights and applications, Phys. Status Solidi B 284 (4) (2011) 775–789, http://dx.doi.org/10.1002/pssb.201046195.

[39] C.J. Cramer, D.G. Truhlar, Density functional theory for transition metals and transition metal chemistry, Phys. Chem. Chem. Phys. 11 (2009) 10757–10816, http://dx.doi.org/10.1039/B907148B.

[40] I.d.P.R. Moreira, R. Dovesi, Periodic approach to the electronic structure and magnetic coupling in $KCuF_3$, K_2CuF_4, and $Sr_2CuO_2Cl_2$ low-dimensional magnetic systems, Int. J. Quantum Chem. 99 (5) (2004) 805–823, http://dx.doi.org/10.1002/qua.10862.

[41] X. Feng, N.M. Harrison, Magnetic coupling constants from a hybrid density functional with 35% Hartree–Fock exchange, Phys. Rev. B 70 (2004) 092402, http://dx.doi.org/10.1103/PhysRevB.70.092402.

[42] I.P.R. Moreira, F. Illas, Ab initio theoretical comparative study of magnetic coupling in $KNiF_3$ and K_2NiF_4, Phys. Rev. B 55 (1997) 4129–4137, http://dx.doi.org/10.1103/PhysRevB.55.4129.

[43] T. Archer, C. Pemmaraju, S. Sanvito, C. Franchini, J. He, A. Filippetti, P. Delugas, D. Puggioni, V. Fiorentini, R. Tiwari, P. Majumdar, Exchange interactions and magnetic phases of transition metal oxides: benchmarking advanced ab initio methods, Phys. Rev. B 84 (11) (2011) 115114, http://dx.doi.org/10.1103/PhysRevB.84.115114.

[44] F. Lebreau, M.M. Islam, B. Diawara, P. Marcus, Structural, magnetic, electronic, defect, and diffusion properties of Cr_2O_3: a DFT+U study, J. Phys. Chem. C 118 (31) (2014) 18133–18145, http://dx.doi.org/10.1021/jp5039943.

[45] H. Noura, GGA+U-DFT+U modeling structural, electronic and magnetic properties investigation on the ferromagnetic and anti-ferromagnetic $BaFeO_3$ characteristics: insights from first-principle calculation, J. Phys. Chem. C 76 (2014) 425–435, http://dx.doi.org/10.1016/j.spmi.2014.10.004.

[46] M. Derras, N. Hamdad, M. Derras, A. Gessoum, New theoretical model on the electronic structure and magnetic properties of the $YMnO_3$ perovskite oxide: implementation of the U-hubbard hamiltonian, Results Phys. 3 (2013) 219–230, http://dx.doi.org/10.1016/j.rinp.2013.09.011.

[47] T. Eom, H.-K. Lim, W.A. Goddard III, H. Kim, First-principles study of iron oxide polytypes: comparison of GGA+U and hybrid functional method, J. Phys. Chem. C 119 (2014) 556–562, http://dx.doi.org/10.1021/jp508096b.

[48] R. Dovesi, R. Orlando, B. Civalleri, C. Roetti, V.R. Saunders, C.M. Zicovich-Wilson, CRYSTAL: a computational tool for the ab initio study of the electronic properties of crystals, Z. Kristallogr. 220 (2005) 571.

[49] I. Gopalakrishnan, N. Bagkar, R. Ganguly, S. Kulshreshtha, Synthesis of superparamagnetic Mn_3O_4 nanocrystallites by ultrasonic irradiation, J. Cryst. Growth 280 (3–4) (2005) 436–441 http://dx.doi.org/10.1016/j.jcrysgro.2005.03.060.

[50] M.D. Towler, N.L. Allan, N.M. Harrison, V.R. Saunders, W.C. Mackrodt, E. Aprà, Ab initio study of MnO and NiO, Phys. Rev. B 50 (1994) 5041–5054, http://dx.doi.org/10.1103/PhysRevB.50.5041.

[51] K. Yosida, Theory of Magnetism, Springer-Verlag, Heidelberg, 1996.

[52] D. Dubal, D. Dhawale, R. Salunkhe, S. Pawar, C. Lokhande, A novel chemical synthesis and characterization of Mn_3O_4 thin films for supercapacitor application, Appl. Surf. Sci. 256 (14) (2010) 4411–4416 http://dx.doi.org/10.1016/j.apsusc.2009.12.057.

[53] H.J. Monkhorst, J.D. Pack, Special points for brillouin-zone integrations, Phys. Rev. B 13 (1976) 5188–5192, http://dx.doi.org/10.1103/PhysRevB.13.5188.

[54] M. Penicaud, B. Siberchicot, C.B. Sommers, J. Kubler, Calculated electronic band structure and magnetic moments of ferrites, J. Magn. Magn. Mater. 103 (1–2) (1992) 212–220, http://dx.doi.org/10.1016/0304-8853(92)90255-M.

[55] W. Li, C.F.J. Walther, A. Kuc, T. Heine, Density functional theory and beyond for band-gap screening: performance for transition-metal oxides and dichalcogenides, J. Chem. Theory Comput. 9 (7) (2013) 2950–2958, http://dx.doi.org/10.1021/ct400235w.

[56] J. Muscat, A. Wander, N.M. Harrison, On the prediction of band gaps from hybrid functional theory, Chem. Phys. Lett. 342 (3–4) (2001) 397–401, http://dx.doi.org/10.1016/S0009-2614(01)00616-9.